Pantelis Butzopulos

Low-Pass Chebyshev Filter based on Integrated Passive Device Technology

Metropolia University of Applied Sciences

Bachelor of Engineering

Electronics

Bachelor's Thesis

23 May 2024

Abstract

Author:	Pantelis Butzopulos
Title:	Low-pass Chebyshev Filter based on Integrated Passive Device
Number of Pages:	30
Date:	23 May 2024
Degree:	Bachelor of Engineering
Degree Programme:	Electronics
Professional Major:	
Supervisors:	Jan Saijets, Project Manager (VTT) Heikki Valmu, Principal Lecturer (Metropolia UAS)

The purpose of the thesis work was to design a Low-Pass filter on an Integrated Passive Device. The work was commissioned by VTT Technical Research Centre of Finland Ltd. The specifications of the prototype design were a pass-band frequency range of 2.2GHz, a ripple of 1.0 dB, and an insertion loss below 1.5dB. The stop-band frequency range was set between 2.8 and 10GHz, with a suppression of 50dB. The aim of the work was to study, design and create an effective filter.

Thesis study dealt with implementation of filters in general, such as passive, active filters and different type of filters. The Chebyshev filter type was the best option to approach this design, due to transmission zeros that makes the response of Chebyshev to decrease the stopband as it goes further. So, the attenuation increases the further it goes upwards from the passband.

In the execution and testing part, the circuit was synthesized by Nuhertz software and continued AWR Software by creating every EM-component step by step. The Em-components were made an EM-structure layout, which is the first model. This first model of the prototype was approached by the iteration method to create another circuit with additional passive components. The reason of the iteration method was to improve the result of the Em-structure layout by adjusting the values of the Em-components and making the correct changes in order to improve the stopband and passband of the filter.

The resulting prototype will be used for different kind of applications by the partners who were involved to this project. Also, information of this study can be useful for VTT, because this prototype made based on IPD topology. VTT owns technology and patents related to IPD topology, and as a result, VTT can use this protype in future projects.

Keywords: Design, Low-Pass Filter, Chebyshev, Stop-band, Passband

---

Contents

List of Abbreviations

5G: Fifth Generation.

ESR: Equivalent Series Resistance.

IL: Insertion Loss.

IPD: Integrated Passive Device topology.

LC: Combination of two components Inductor and Capacitor.

LPF: Low Pass Filter.

MIM: Metal Insulator Metal.

MMIC: Monolithic Microwave Integrated Circuit.

NI AWR: National Instrument-Applied Wave Research.

Q: Quality factor.

RC: Combination of two components Resistance and Capacitor.

RL: Return Loss.

S-parameters: Scattering parameters of S11, S12, S21, S22.

VTT: The words are in Finnish and mean National Technical Research Institute.

1 Introduction

This thesis presents a prototype Lowpass Filter (LPF) design based on an Integrated Passive Device (IPD) topology. This design aims to implement an effective filter on IPD topology with a pass-band frequency range of 2.2GHz, a ripple of 1.0dB, and an insertion loss below 1.5dB. The stop-band frequency range is set between 2.8 and 10GHz, with a suppression of 50dB relative to the pass-band edge.

The design was developed at VTT, Finland's largest research and technology company. VTT is engaged in various fields of technology, Finnish business, and society. The state-owned company was established on Jan 16, 1942, and since then, it has made a noticeable impact in every field with the innovation role that it provides. The budget of VTT is approximately 261 million with an employee number of 2213.

The filter was designed using NI AWR software, suppressing different techniques provided by NI AWR to achieve the best possible result. The goal schematic was synthesized with iFilter, and the EM layout was designed step-by-step by, replacing each lumped component with a respective EM structure using AWR AXIEM in IPD topology, and implementing the correct size of capacitors and inductors. To approach the perfect result, iteration and optimization methods were applied to the filter. The filter prototype was approached with Chebyshev, which successfully satisfied the desired specification.

2 Implementation of Filters

2.1 Active Filters

Active filters are used for amplification by using different active elements, such as operational amplifiers, and passive components, such as capacitors, resistors and inductors. Gain can be provided through operational amplifiers and depending on the location of a capacitor, an operation amplifier can display the performance of an inductor. [2, 592.] At low frequencies, the inductance values are typically so high that it is impractical to make a planar coil. If a stated impedance level is to be supported, the inductance values must be extended, and the desired frequency range must be reduced. However, these values can be implemented by expanding the number of turns and applying high permeability of ferromagnetic cores. In addition, the resistance, size and cost of the induction element are increased; therefore, the Q factor is decreased. Active filters are not well suited to RF frequencies due to the frequency limitations of operational amplifier. Similarly, they suffer from linearity problems and are mainly suitable for low-power receivers, but on the transmission side, they lack linearity and introduce too much distortion into the signal. [3, 1-23.]

2.2 Passive Filters

Passive filters can be illustrated simply by capacitors, resistors and inductors [2,589]. The connection between capacitors and inductors is propulsive to create voltage dividers that differ with frequency, due to differing impedance of capacitors. [1, 35]. Passive filters have been developed and evolved since the 1920s, and since then they have been important for communications [3, 1-23].

The low-pass filter allows frequencies below a cutoff frequency and avoids all the frequencies above the cutoff [2,588]. As shown below, Figure 1 represents

a standard low-pass RC circuit in series.

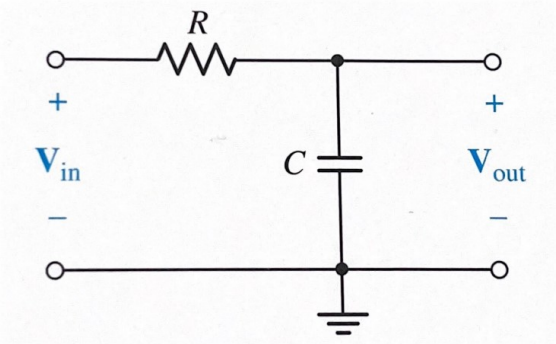

Figure 1. Low-pass Circuit [2].

The model in Figure 1 with a single resistor and capacitor is given the following transfer function and it can be illustrated as

$$H(s) = \frac{v_{out}}{v_{in}} = \frac{1}{1 + RCs} \tag{1}$$

Furthermore, a high-pass filter would be implemented in the opposite order from the LPF to allow high-frequencies to pass through but at the same time discard low-frequencies [2, 589]. The Figure 2 represents a standard RC high-pass circuit [5, 589].

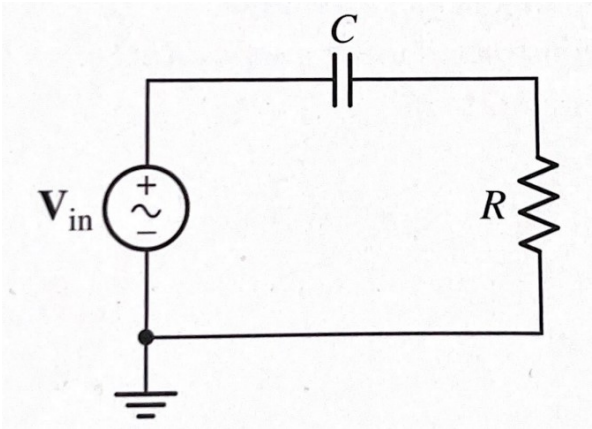

Figure 2. High-pass Circuit [2].

The model in Figure 2 with single a resistor, capacitor, and voltage source can be represented with the following transfer function, such as

$$H(S) = \frac{v_{0Ut}}{v_x} = \frac{RC_s}{1 + RC_s} \tag{2}$$

Subsequently, a band-pass filter is coupled with a low-pass and high-pass filter to allow an accurate frequency segment; the rejected frequency range is indicated as a stop-band filter. [2, 588.]

As shown below, Figure 3 illustrates a standard RLC band-pass circuit.

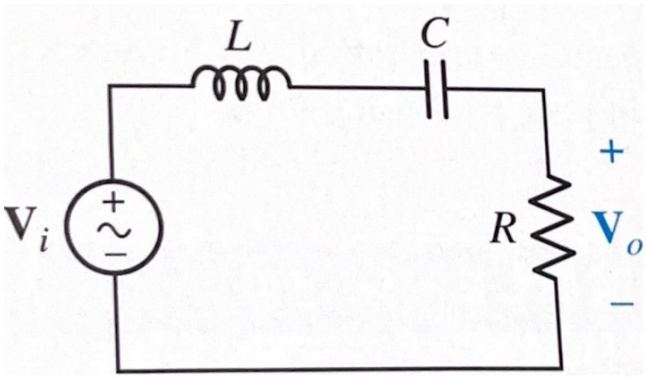

Figure 3. Band-pass Circuit [2].

The frequency response in the pass band cannot be constant, which means that at high frequencies the magnitude response must have some sort of limit. The same happens in the stop-band side, which is the inverse of the pass band. [5, 398.]

As shown below, Figure 4 represents all the different types of filters that were covered above within cut-off frequencies.

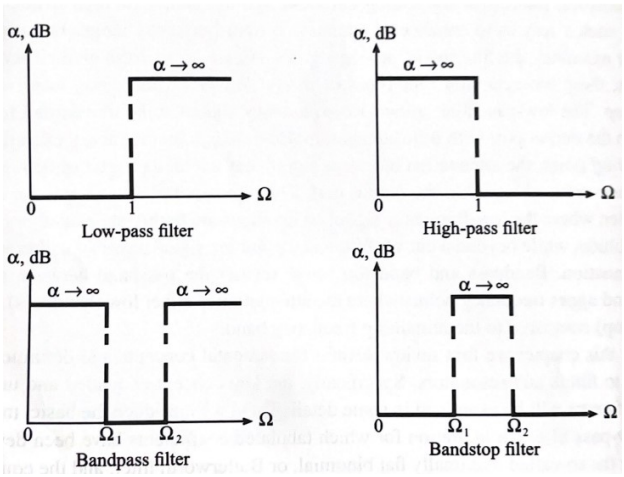

Figure 4. Cut-off Frequencies [6].

Figure 4 shows the attenuation α as a function of the angular frequency of the different filter types. The Ω presents as a parameter for the normalized frequency regarding the angular frequency. The cut-off frequency for low-pass and high-pass, respectively, is included in Ω. Lastly, the band-pass and band-stop consist of the centre frequency. [6, 202-203.]

2.3 S-Parameters

S-parameters have developed especially for high frequencies such as RF and mm-waves because measuring, propagating and reflected signal power is more practical than the current and voltage measurements required by Y- and Z-parameters at high frequencies. S-parameters show the electrical behaviour of a network called the frequency domain. S-Parameters are determined by the magnitude and phase. These parameters are affected by input signal that depends on the network from losses and reflections. S-parameters define ports, and the characteristics of linear networks can be calculated using them — for example, gain, loss, impedance, phase and voltage standing wave ratio.

The two-port parameters are defined with input and output variables. S11 is the input reflection coefficient, S21 is the gain, S22 is the output reflection coefficient and S12 is the opposite of the transmission. [17, 139-140.]

2.4 Two-port Network

The two-port network has input impedance, a function of the load value. Correspondingly, the value of the source is a function of the output impedance. [9, 153.] Two-port networks are specified as the frequencies of zero transmission to receive zero output for a finite input. In order to have zero transmission in a two-port network, the signal must be blocked from input, and the transmission paths shorted. Different approach is to halt the signals at the output that are transmitted from various paths. [3, 8-1.] As shown in Figure 5, this two-port network is included with Zs as the terminated source and ZL as load impedance. As well as Pin is the power generator, Pr is the reflected power, and Pout is the filter at the output. [8, 227-228.]

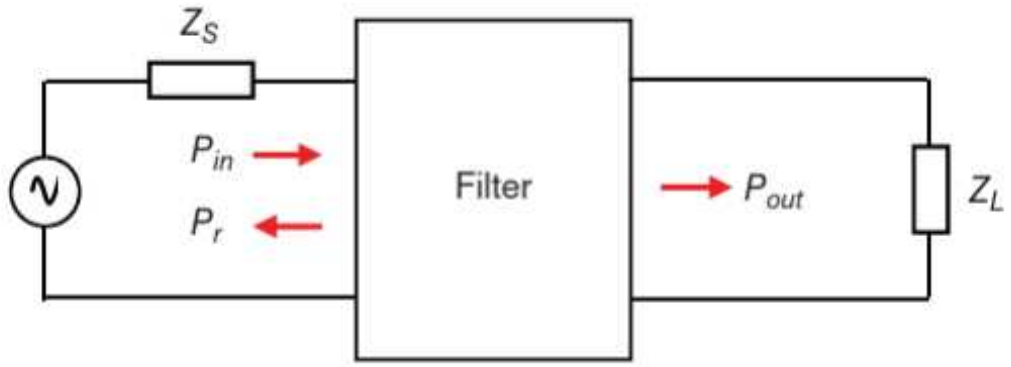

Figure 5. Two-port Network Filter [8].

The performance of a filter depends on different parameters. The insertion loss (IL) appears, when a filter is added into a system, which results in receiving the quantity of reflective losses [8,228]. The insertion loss can be illustrated with the equation (3).

$$IL = 10log\left(\frac{P_{out}}{P_{in}}\right) dB \tag{3}$$

The return loss is generated in a specific filter port as a result of the loss of reflections [8, 228]. The return loss can be illustrated with the function (4)

$$RL = 10log\left(\frac{P_{in}}{P_r}\right) \quad (4)$$

2.5 Chebyshev Filter

Generally, implementing attenuation that displays the binomial filter to accomplish the attenuation transition from passband to stop-band demands many components. In Chebyshev, the ripples are managed at the same amplitude level as the stop or pass bands. [6, 203.] Chebyshev is amused with a demand for an excellent cut-off. The insertion loss particularly impacts filter's performance. [10, 419]. However, the passband activates the progression of the Chebyshev filter to become steeper than the Butterworth. Furthermore, Chebyshev is more successful on lower-order filters, but the phase response is not linear enough. [13, 27.] Figure 6 illustrates a sketch of the Chebyshev low-pass filter response, where Lr is the pass-band ripple in dB, f is the frequency, and fc is the cut-off frequency [8, 237].

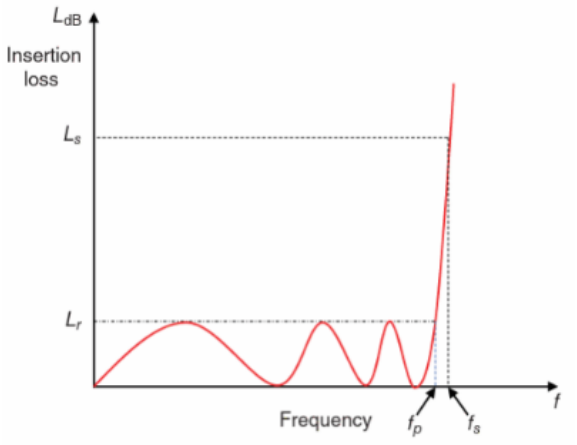

Figure 6. Chebyshev Low-pass Filter response [8].

Two different types define Chebyshev. The type I filter has a sharper transition and grants a certain amount of ripple in the pass-band or the stop-band. Figure

7 demonstrates the frequency response of a seventh-order Chebyshev type I filter, which is required to succeed in the pole-zero configuration. [15, 11-12.]

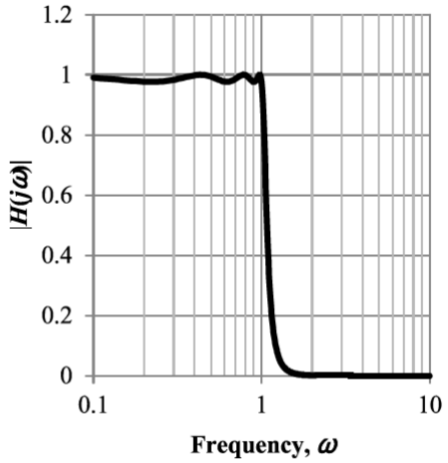

Figure 7. A seventh-order Chebyshev Type I Filter Frequency Response [14].

Moreover, the Chebyshev Type II filter's stop band can possess a ripple while the pass band is monotonic. Figure 8 demonstrates the frequency response of a seventh-order Chebyshev type II filter, where the poles are the reverse of the poles of the type I filter. [15, 13-14.]

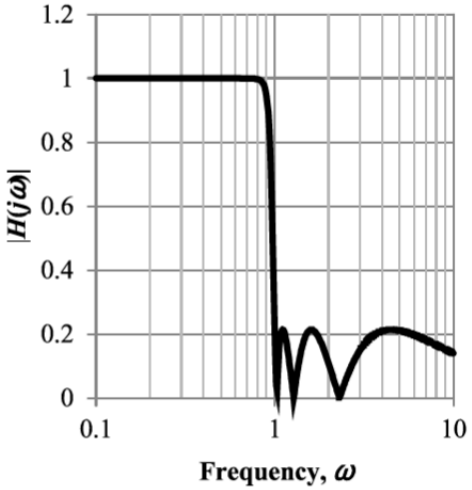

Figure 8. A seventh-order Chebyshev Type II Filter Frequency Response [14].

2.6 Butterworth Filter

Butterworth is the most fundamental filter; its response is also known as a flat response [12, 150]. The flat response is known for the smoothness through the passband to the stop-band. Also, the response is affected by a poor roll-off. [13, 19.] Butterworth filters are performed perfectly with analogue-modulated gestures. [8, 230]. The all-pole transfer function included with no finite zeros in the lowpass Butterworth polynomial [13,19]. A sketch of Butterworth filter response with second and fourth order is illustrated in Figure 9.

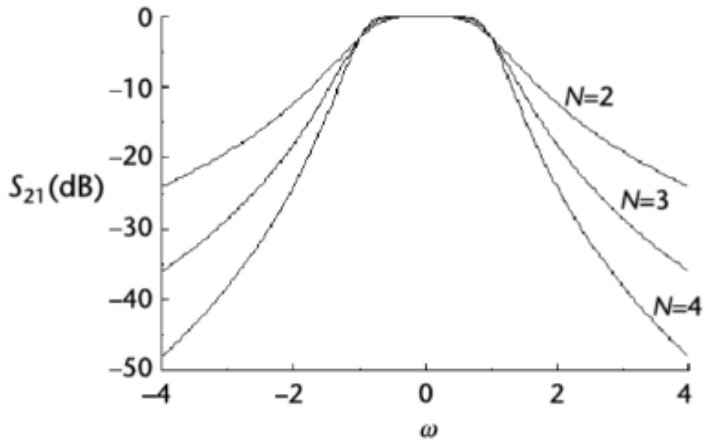

Figure 9. Comparison Butterworth response [11].

2.7 Elliptic Filter

The elliptic filter after the cut-off frequency provides a better-lifted skirt of selections than Chebyshev. However, the elliptic filter can become more complicated because it is required to use shunt or series resonant elements or cross-coupled elements between nodes, regarding Chebyshev and Butterworth filter uses non resonant elements. [12, 168-169.] A frequency response of a fifth-order elliptic filter is represented in Figure 10.

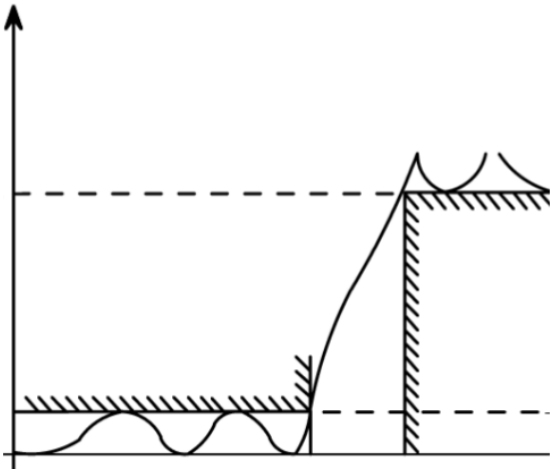

Figure 10. A fifth-order elliptic filter response [11].

2.8 Bessel-Thompson Filter

The Bessel Thompson filter is developed for flat group delay over the pass- and transition-bands. At the same time, the bandwidth of the output spectrum is restricting. This filter is expansive in different kinds of measurement systems and communication as well. The falsification of pulse shapes and other short-term waveforms is significant. [15, 41.] The group delay characteristics for the Bessel-Thompson filter, when n=1,2 and 3, are represented in Figure 11.

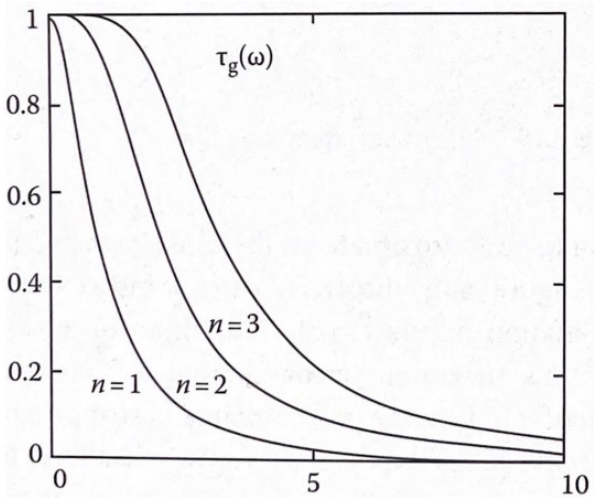

Figure 11. Group delay characteristics for the Bessel-Thompson [3].

2.9 Lumped-Element Components

There are many kinds of methods that are usable in high-frequency circuits. Resistors apply carbon compositions to the immune element, and it can be applied to any type of package configuration. As the frequency rises, parasitic packaging will be brought to the resistors.

A lumped capacitor is a simple growth of the parallel-plate capacitor. It is included with counter parallel conducting plated detached by a dielectric. The capacitance can be illustrated with the below function (5)

$$C = \frac{\varepsilon A}{d} \tag{5}$$

ε is the symbol of dielectric permittivity, then A refers to the plates' area, and d is the distance between them. Capacitors can be used as a planar or chip layout at high frequencies. The most popular materials are ceramic and mica. The Q called the quality factor, is involved in the accomplishment of the capacitor; below the function (6) contains the Q of a series resonant circuit.

$$Q = \frac{1 \,/\, \omega C}{R} = \frac{1}{\omega C R} \tag{6}$$

The C is capacitance, and R is the resistance of the effective series (ESR).

A circular model of coil represents an inductance. Below is illustrated an inductance function (7).

$$L = \frac{0.394 r^2 N^2}{9r + 10l} uH \tag{7}$$

The r represents the radius of the coil, N is the number of turns on the coil and l the length of the coil. Important parameters affect the inductor, such as the

capacitance between the N (turns) of the coil and the series resistance. The skin effect is affected by the resistance of the conductor, and it can be grown with frequency. [8, 159-163.]

2.10 Planar Components

The design process of a filter can become complicated. The implementation of a simple layout spiral inductor is included by the conducting track, which is a spiral model, square, circular, or hexagonal. The input of the spiral is designed to connect with the inner of the spiral by a dielectric overlay. This overlay is designed by a strip that passes over the turns of the spiral inductor, as illustrated in Figure 12, and the conductor is printed over this strip to connect the inner end of the spiral. The technology of this track is a thick film.

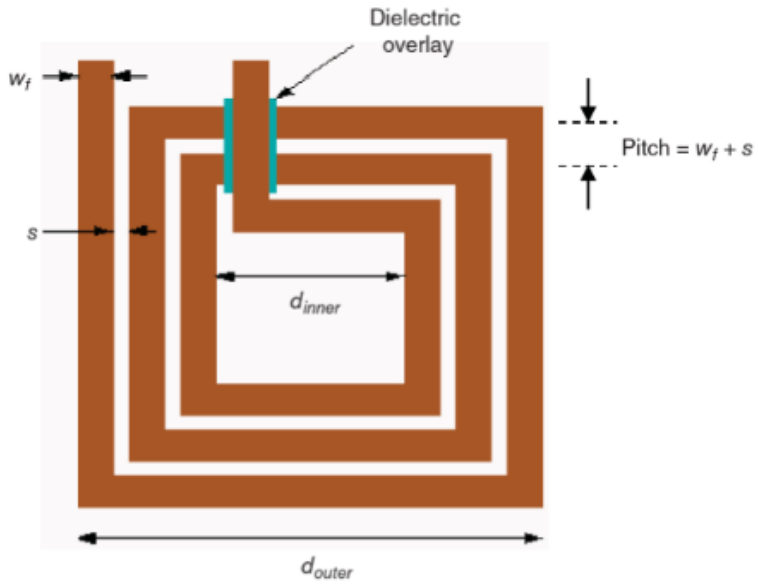

Figure 12. Spiral Inductor [8].

A spiral Inductor is performance self-capacitance counting the capacitance between turns and the ground. The inductor develops series resistance by the number of turns and thinness of the track, as well as self-resonant frequency. The shape and dimensions of the spiral can have a significant role in the

performance of the inductor. Circular models usually perform significantly better. [17, 47-50.]

Furthermore, in some cases, inductors must be tiny in order to achieve the desired inductance value. This model of inductance is called a loop inductor and Figure 13 below represents a loop inductor, where r is the radius of the loop, and w is the width of the track.

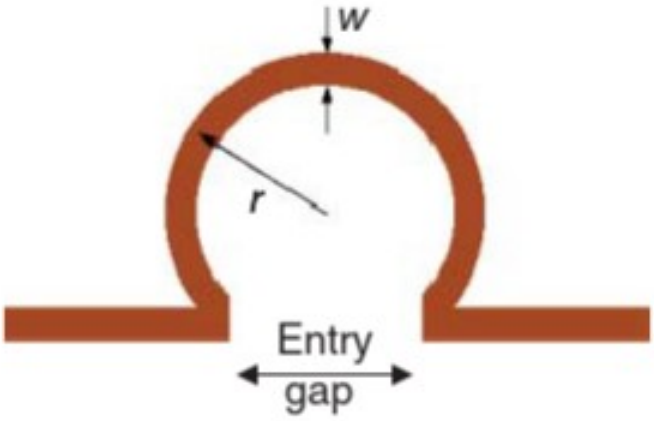

Figure 13. Loop Inductor [8].

The entry of the loop is designed to be with the size of the gap 5w to bypass undesirable capacitance. Also, the spiral inductor has higher self-capacitance than a loop because of the capacitance per unit length of the conductor. On the other hand, the self-resonant frequency of the spiral inductor is lower than that of a loop inductor. [17, 50-52.]

Next, the structure surface of interdigitated capacitors has two metallic conductors, where are coupled by several fingers. Fingers form a large-distance coupling gap, although their widths and spacing are the same. This kind of model is applied for different kinds of use, such as in MMIC (Monolithic Microwave Integrated Circuit) and in hybrid circuits. The total capacitance of the structure can be calculated with the function (8) below. [17, 37-38.]

$$C = (\varepsilon r - 1) l [N - 3]\, A1 + A2] pF \quad (8)$$

The model in Figure 12 below can be represented with the function above. The εr is symbolized the dielectric constant. The l is finger's length overlapping in μm, N is the number of fingers, and A1 and A2 are the modification factors. According to Figure 14 below, these functions are factors of h/wf; the thickness symbolized by the h, and wf the width of the fingers correspondently. [17, 38-39.]

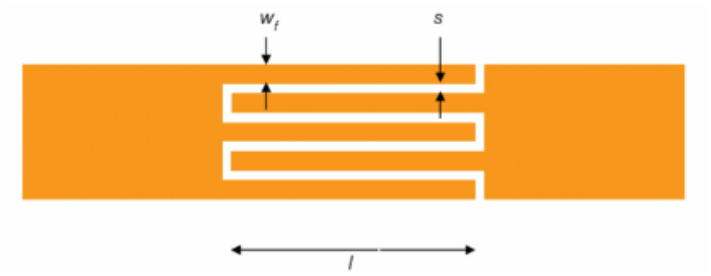

Figure 14. The Interdigitated Capacitor [8].

The finger's width ratio (wf) and the gap size (s) can be raised by Q-factor. [17, 40-41.] There are some cases where the capacitance must be larger than the given value. The MIM (Metal Insulator Metal) capacitor is excellent for these cases. Figure 15 represents the dielectric part overlapping the open-end of the microstrip and shaping the lower part of the capacitor. In addition to forming the upper electrode, a separate microstrip line is added over the dielectric.

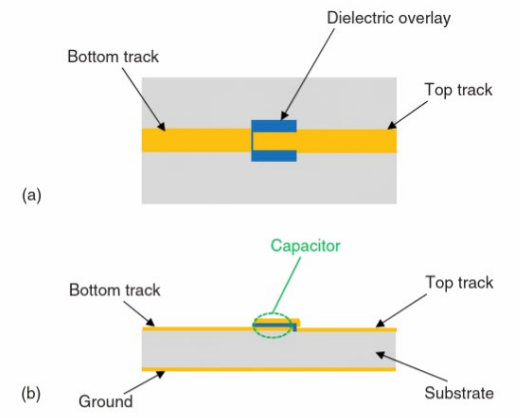

Figure 15. MIM Capacitor: (a) upper and (b) side view [8].

The Q-factor is high, and so the resistance of the dielectric between the electrodes. The electrodes have their resistance, which can cause an ohmic loss. The technology is a thick film, meaning that the capacitance value can be adjusted by changing the structure. [8, 168-169.]

2.11 Integrated Passive Device

IPD technology is a leading LC filter technology universally in 5G systems. IPD is advanced with small-scale device height and semiconductor process. The capacitors are developed on a thin film to have high capacitance density above 3 GHz. The high capacitance density provides a small-scale capacitor which is beneficial for less parasitic resistance and inductance. The Q-factor and resonant frequency are suitable, and the grater is displayed by the MIM capacitors. Also, IPD technology is suitable for large bandwidth, less loss, and small-scale filtering results. The material of the wafer is a demanding part of the accomplishment of the IPD filter. Different types of material such as silicon IPD or glass IPD, provide an excellent result for RF delivery because of the advanced resistivity and reduce of dielectric constant of glass. [19, 13-16.]

A band-pass filter applying a thin-film IPD technology on a silicon surface is represented in Figure 16. The side view of the structure is illustrated by two metal layers, M2 and M3, which are made of polyimide. A third metal layer, M1, and is connected to the bottom electrode side of the capacitors. The inductor coils are placed at the top layer, which is an 8-um thick layer of copper. There are two aluminium bottom layers. The surfaces are developed to have less loss and, at the same time, to be influenced by the quality factor of the inductor at high frequencies. [20, 2.]

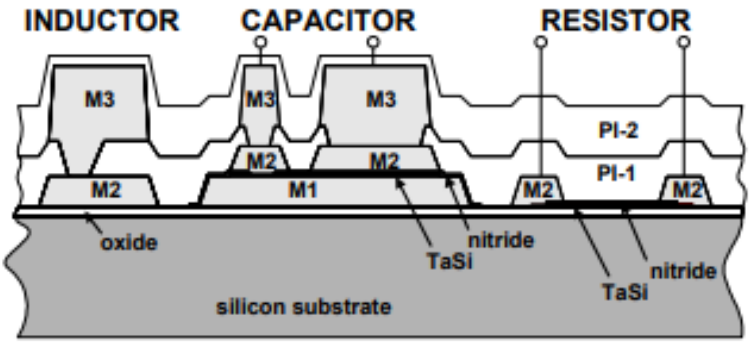

Figure 16. The cross-view of IPD Structure [19].

It is particularly important to compare the inductance and quality factors for the desired result and maximum filter performance. Two cases where a comparison between inductance and quality factor has been made are shown in Figure 17 below. The peak Q value of the 1-ended coil is reached at around 2GHz and the self-resonance at around 10.5GHz. The self-resonance of a differential structure is at a much higher frequency than that of a 1-headed structure. [20, 2-3.]

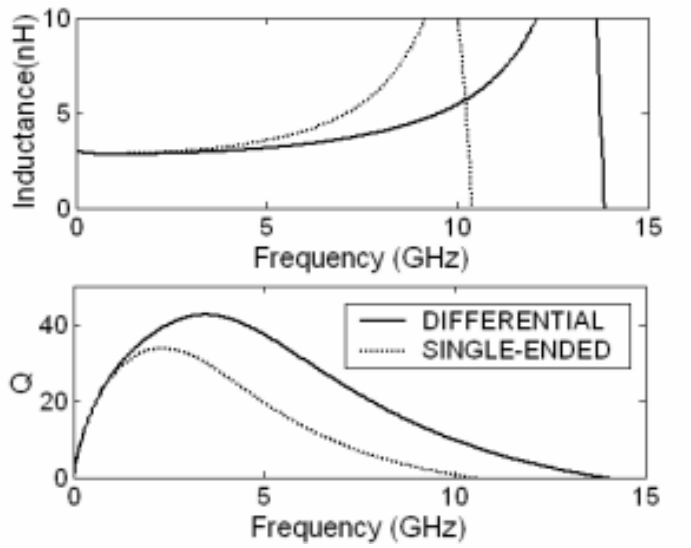

Figure 17. IPD Inductor: Upper Inductance and beneath Quality Factor [19].

3 Execution and Testing

3.1 Schematic

The thesis aimed to implement a low-pass filter based on integrated passive device topology. The pass-band frequency range was 2.2GHz, with a ripple of 1.0dB, and an insertion loss less than 1.5dB. The stop-band frequency range was set between 2.8 and 18GHz and the suppression was 50dB relative to the pass-band edge.

The implementation of the design was done with NI AWR software. To achieve these specific specifications, it was necessary to approach and research all the filters that are possible candidates. In the theory part (chapter 2.5; 2.7), both Chebyshev and Elliptic can provide excellent cut-off frequency, as stated in implementation of filters [10, 419; 12, 168-169]. The design was approached with a modified Chebyshev filter approach because the schematic was shorter than Elliptic, so less complicated. The transmission zeros add to transfer rollers more steepness to the edge of the emission band.

The Chebyshev filter was synthesized using NuHertz software by adding two finite transmission zeros to the primary Chebyshev filter at the beginning of the stopband. The aim was to minimize the order of the filter and get the best possible balance between the attenuation of the transmission and a steep roll-off. The order of the filter was limited to 7 to minimize losses. However, two finite transmission zeros at 2.85 and 3.6GHz were placed at the beginning of the stop band to achieve sufficient attenuation steepness at the beginning of the stop band. Figure 18 presents the synthesized 7^{th}-order Chebyshev schematic and the graph, where the passband frequency is 2.250GHz, the passband ripple is 0.15dB and the schematic contains stopband zeros. The schematic is designed with simple lumped passive components with two ports of 50ohms. The graph represents the simulated result of the theoretical schematic with excellent passband and stopband. The y-axis is the insertion loss with a range of 0 to -80dB, and the x-axis is the frequency with a range of 0.001 – 10GHz.

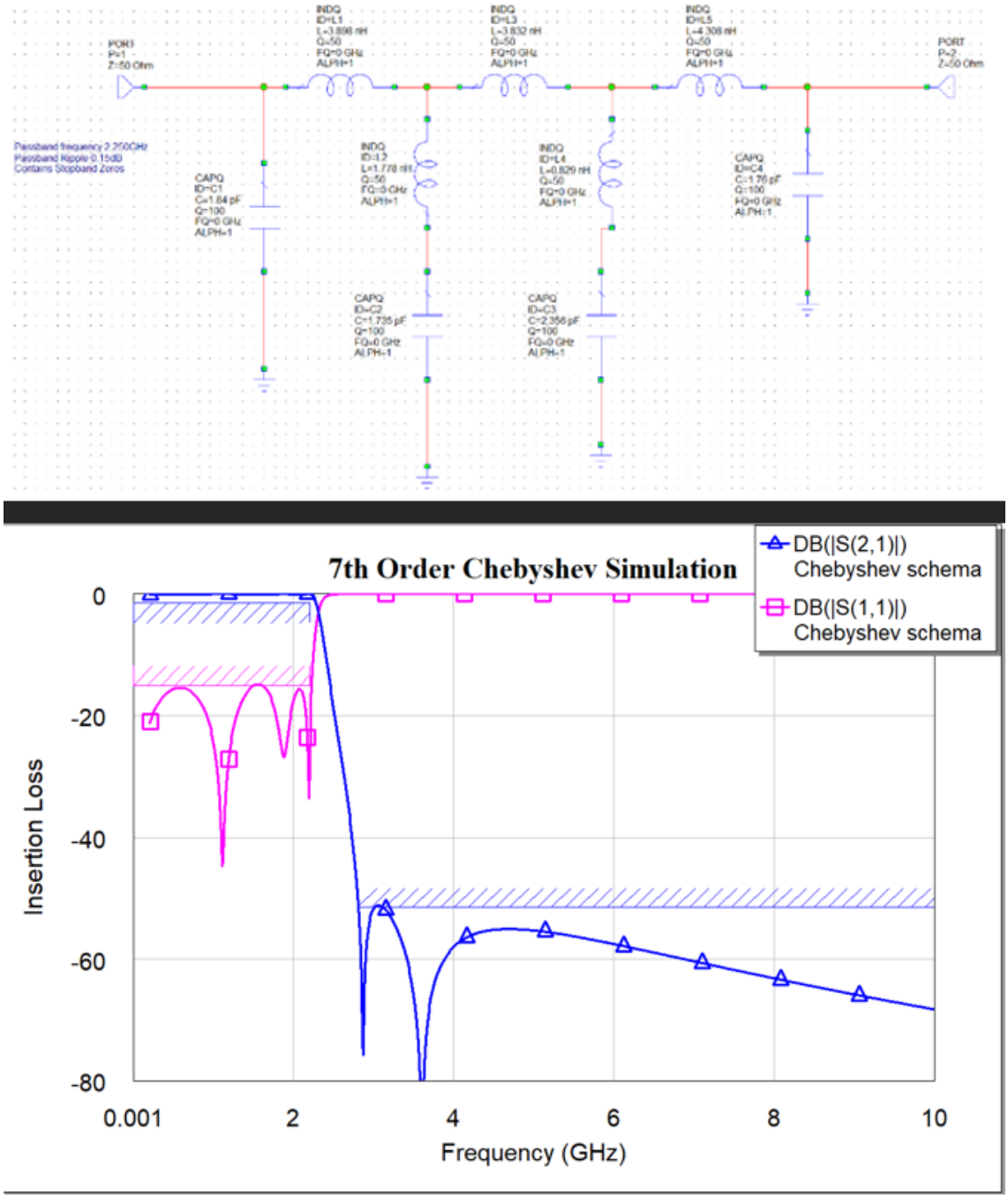

Figure 18. 7th Order Chebyshev Schematic with ideal components and its simulated response.

3.2 Subcircuit Schematic

One of the most important aspects of the search for the theoretical target scheme was to find L and C values that can be produced by IPD technology. The aim was to design each lumped IPD component using 3D simulations in

AWR AXIEM and replace the schematic components with EM subcircuit blocks to ensure the wanted response. VTT's IPD technology uses three copper metals, hires silicon wafers as substrates and can be used to make coils, capacitors, transmission lines, and other planar RF components (e.g., antennas, baluns). In VTT's IPD technology, the capacitance is determined by the thickness of the dielectric layer between M1 and M2 and the surface area between their metals. Implementing the correct size of capacitors and inductors was very crucial, as stated in theory part (chapter 2.11), to achieve the exact value as was in the lumped passive schematic [19, 13-16]. Figure 19 represents a spiral inductor with a number of turns of 2.5, a width of 20um, a distance of 15um between the spiral lines, and an inner radius of 100um. The value of the spiral inductor was adjusted by changing mainly the radius value and number of turns if necessary. As stated in the theoretical part (chapter 2.10), the blue line symbolizes the bridge or dielectric overlay that helps for the continuity of the signal. The blue line is the M1 layer, the yellow line is the M3 layer, and the red pads are the M1-to-M3 via-stacks.

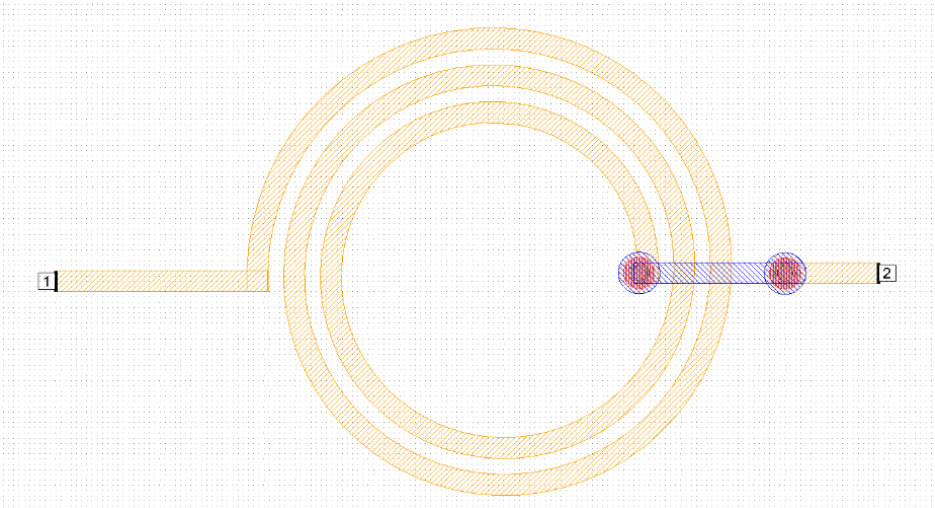

Figure 19. Example layout of a Spiral Inductor.

Furthermore, the same approach was taken to MIM capacitors as well. The value of the capacitors was adjusted by stretching the EM component. Figure 20 presents a MIM capacitor. The MIM capacitor has two metals, one thick and one slim. The stretch must be done horizontally according with the Figure 20 or

vertically on thick metal side. The stretch must be done carefully and precisely to keep the structure in correct form without damaging it. The capacitors also contain M3 layers on yellow lines; M2 layer is the red space metals that are connected in between with a blue dielectric overlay bridge at the M1 layer. Upper red area defines the MIM-capacitor area that is formed between M1 and M2 whereas the lower red area is simply M1-to-M3 via-stack connecting the M1 bottom plate to M3.

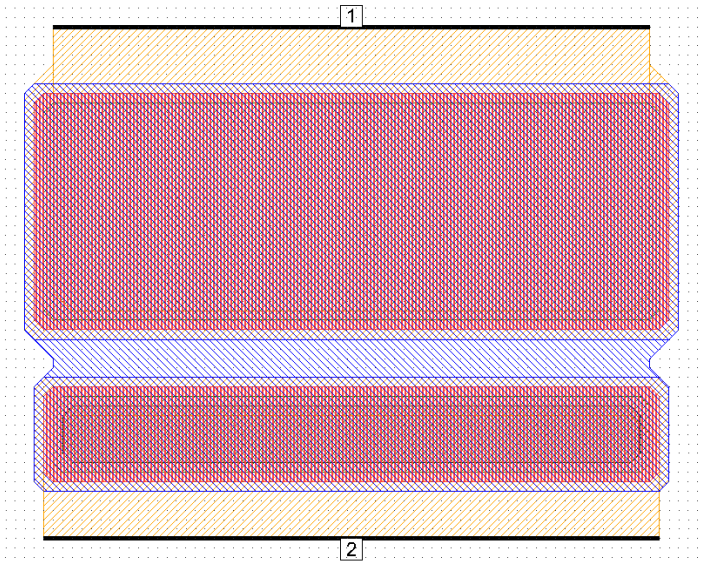

Figure 20. Example layout of a MIM Capacitor.

Furthermore, the creation of every Em component is illustrated on Figure 21, where every lumped component has been replaced from subcircuit, in which every subcircuit contains its own Em component. Figure 21 presents the subcircuit schematic with two 50-ohm ports. The subcircuit can be changed simply by clicking next to the subcircuit and choosing different EM components that have been created in AWR software. The graph represents the result of the schematic, and there is a slight difference in passband compared to Figure 18. The reason of this difference is mainly the size of the inductor's spirals. In this part, the important concept is to receive precise results, which will help later to build the EM structure layout. Although the passband and stopband remain in the desire specifications, the passband is a bit above the S11 brown line. On

the other hand, the stopband is a perfect result that remains under 50dB and, at the same time, creates a spectacular cut-off frequency.

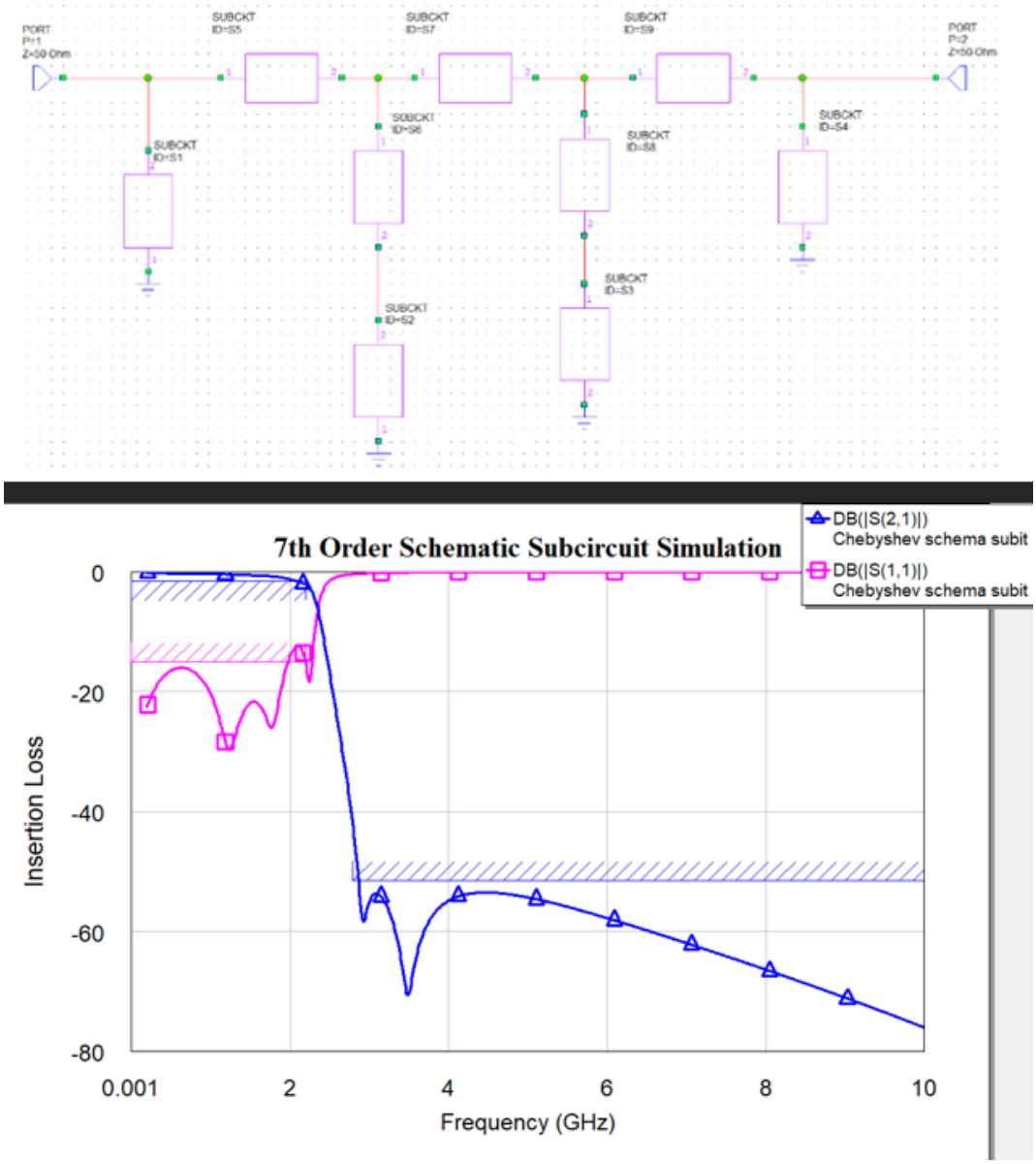

Figure 21. Subcircuit Schematic and Result.

Additionally, the creation of every subcircuit of the EM component must match the value of the lumped components correspondently. These values are important to be accurate, because the graph must be as close as possible to the lumped passive components schematic. Figure 22 represents two graphs, where on the left-hand side spiral inductance presents all the spiral EM

components, and on the right-hand side is the capacitance of the capacitors. The identification of the desired values happens in the y-axis. This plot is therefore the value of inductance and capacitance extracted from the EM simulation (Z and Y parameters). The graph shows the frequency range in which the component operates at which value. The y-axis represents the values of the Em-components, and the x-axis represents the frequency.

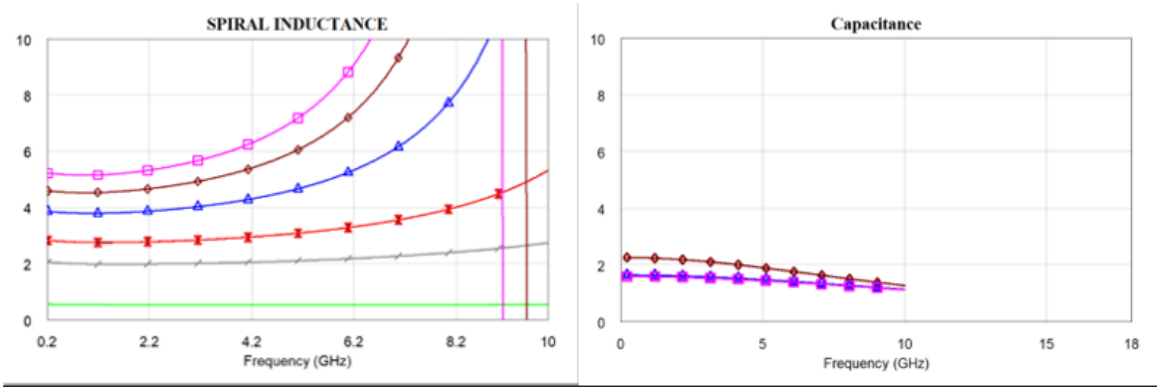

Figure 22. The Values of Inductors and Capacitors.

4 Testing and Results

4.1 First Model of Chebyshev Filter

After the design of the individual components, they were assembled according to the schema. The Em components were placed in the same position as were in the lumped passive schematic to achieve correct functionality. The distance between every component was in a specific range of around 300-350um, and the pitch between the inductors and capacitors around 70um. The design was designed to be measured with a 150 µm pitch ground-signal-ground head structure. In the EM simulation, 50-ohm gates were placed on the heads. The layout was surrounded by ground plate, where the capacitor's thick metal side connected the whole design had a total diameter horizontally of 3.583mm and vertically 1.945mm. As shown below Figure 23 is designed similarly to the lumped passive components schematic; the design was the first model of the prototype lowpass Chebyshev filter. The first and last inductors were flipped in

order to the currents go in opposite directions in the coils so that cross-coupling is minimised and does not interfere with the operation of the components and reduce the barrier band requirement. Many factors affect the circuit, such as isolation structure around the circuit (ground) and electromagnetic field distribution.

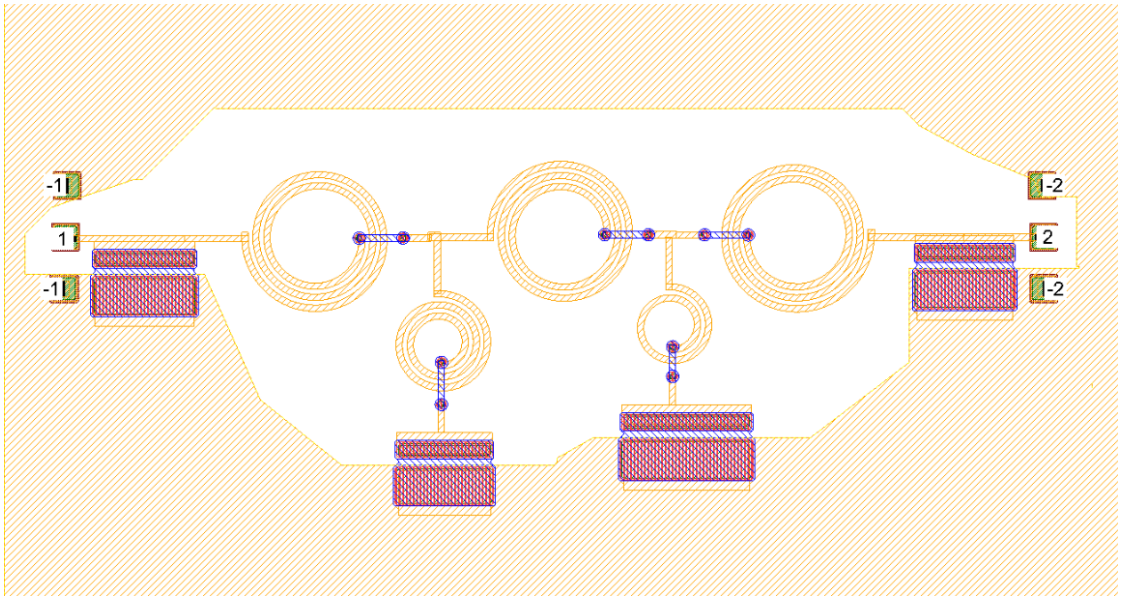

Figure 23. The First Model of Chebyshev Filter EM Layout.

The simulated response of the above EM layout is represented in the Figure 24 below, where the stopband was like Figure 18 as expected, with a perfect cut-off and below the desired specifications. On the other hand, the passband reflections were slightly above the desired specification. This is rather a normal response at this design phase, because real 3D components cannot give exact same results with the theoretical ideal components. The circuit on the EM-side can be affected by parasitic effects, boundary conditions and coupling between the components. However, this reflection response that is shown in Figure 24 below can be fixed and optimized by combining the EM structure with theoretical small L and C tuning components.

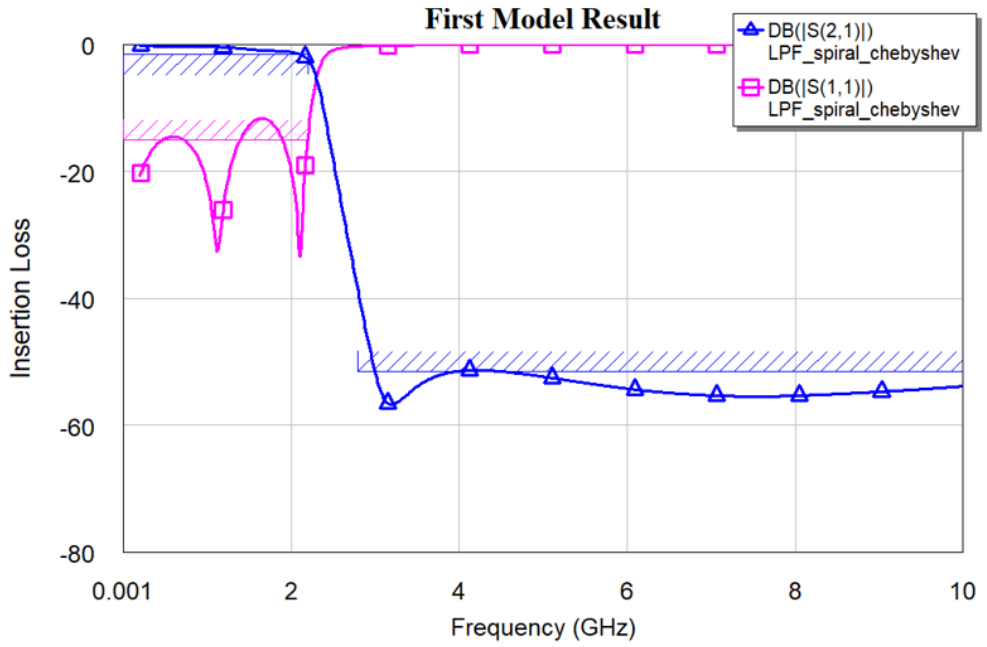

Figure 24. Simulated S-parameters of the full EM layout of Figure 23.

4.2 Method of Iteration

As mentioned above the filter transmission and reflections responses can be improved by iteration. The idea was to know the value of each component and see what kind of change the component requires. The tuning ports are placed on the layout so that the tuning ports of the desired coil are made by cutting the coil and placing the ports in series. The two ports of the capacitors are placed over the capacitor for parallel connection. On the circuit side, these are used to place tuning components which, at 0, correspond to the EM simulation without gates., as shown in Figure 25. The ports must be placed correctly and preferably on the same spot of every component in order to be accurate on the adjustments.

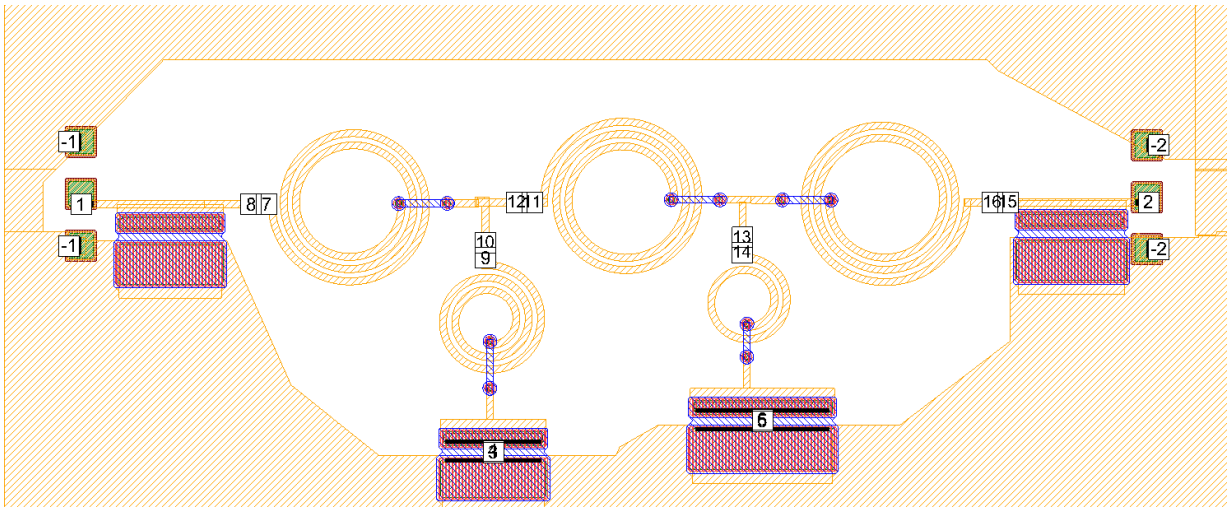

Figure 25. Modified EM layout for components value tuning.

Tuning of the components of the EM structure was done with circuit diagram in Figure 26, where the value of each component can be adjusted upwards or downwards. The inductors are named L1c-L5c, and capacitors C1c-C4c correspondingly. The component values were tuned with the tune tool of AWR software. The tuning tool helped to adjust the values of the components and watched the stop- and bass bands' behaviour in real-time. The new values were not 100% accurate because as mentioned above, the components on the EM-side behave differently than in the lumped passive element circuit side. The new EM-component values of these corrections C1c-C4c and L1c-L5c, were constrained by +/-50% of their absolute value.

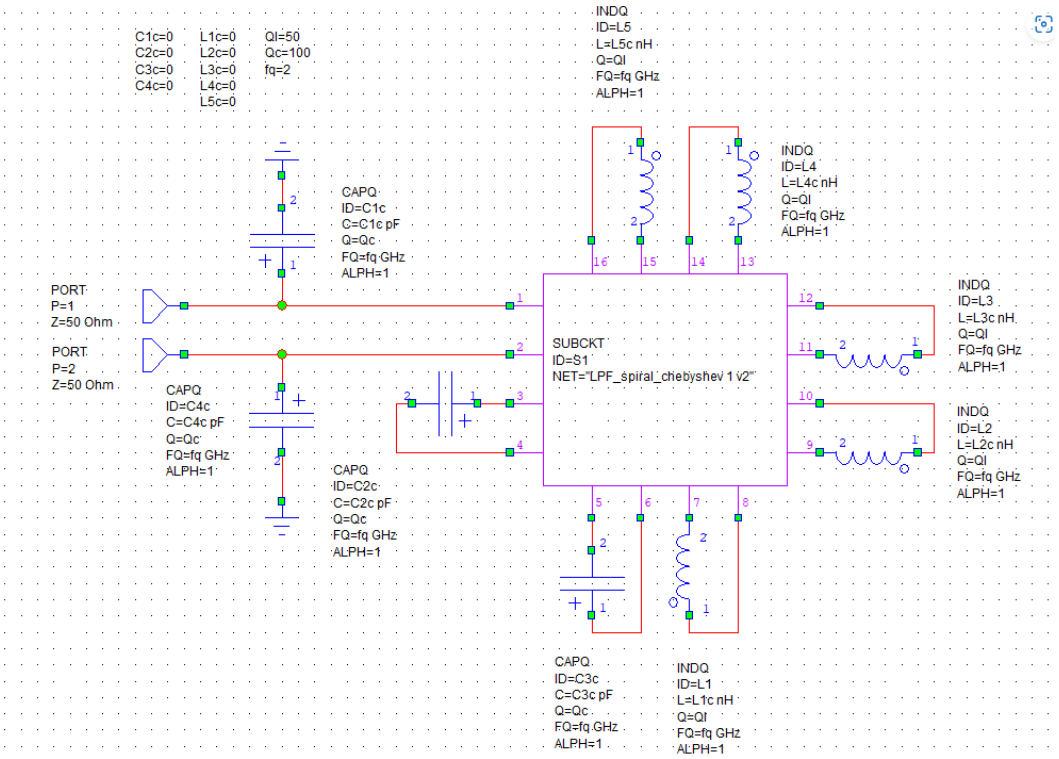

Figure 26. The subcircuit for tuning EM component values.

Based on the tuning of the circuit simulation, the EM components were resized in the direction indicated by the circuit simulation/tuning. In addition to being precise with any change on EM layout components, it was practical to create a few choices for every component. The models were named “decrease” for decreased and “increase” for increased value compared with the original new value. The reason for that was to follow the behaviour of every component on the EM-layout side as the result to correct the reflections errors and other possible errors. This method can improve the graph but does not guarantee that it matches the desire specifications. However, the creation of “decrease” and “increase” components can improve the pass- and stop bands even more.

4.3 Final EM Model of Chebyshev Filter

This design’s final model was made by repeatedly changing the sizes of almost every component with the “decrease” and “increase” choice models. The total time of every simulation was approximately 40 minutes. As shown in Figure 27

below, the final model appeared to look like the first model in Figure 23. The order of every component remained the same as well as the GSG pads with the two ports. The shape of the ground inside this close circle is modified to be as much as groomed as possible, so as not to block or bother any signal that is transmitted.

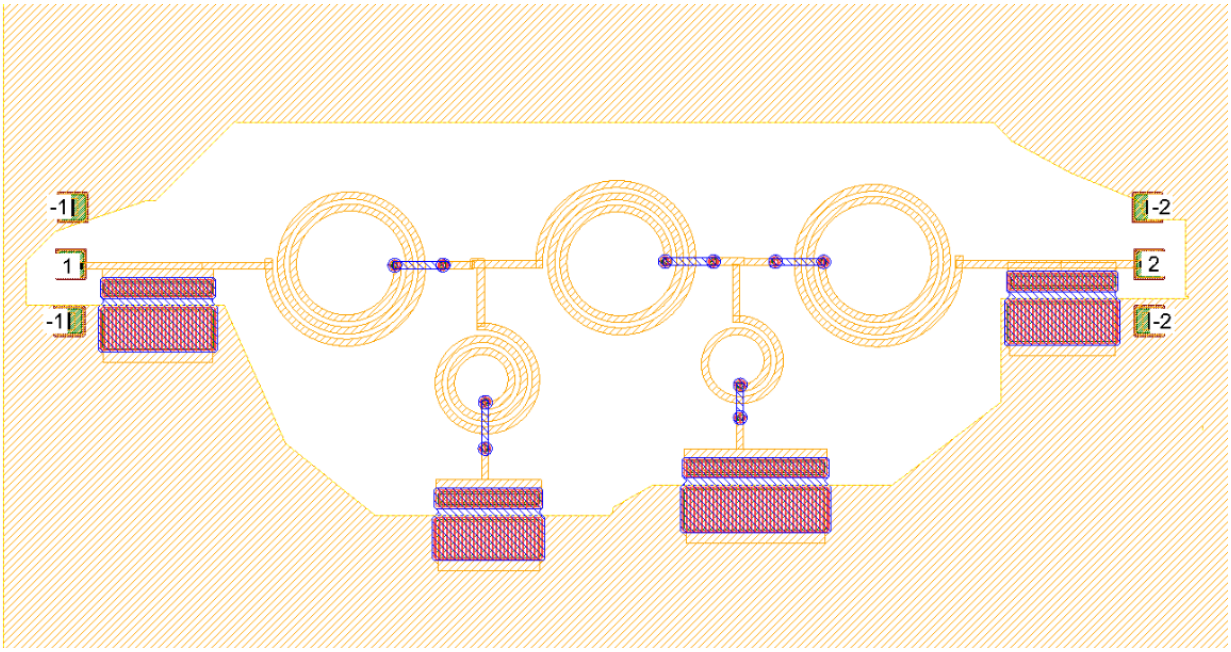

Figure 27. Final EM layout of the lowpass Chebyshev Filter.

Figure 28 shows the final simulation result of the above EM-layout, where the S21 with blue line symbolizes the ratio between the transmission signal and that is called forward transmission coefficient. S21 shows that the insertion loss in the pass band below 2.2GHz is less than the specified maximum loss and that attenuation increases sharply after the cut-off frequency and reaches the blocking band requirement at 2.8GHz. Also, the S11 as a pink line is the input port reflection coefficient or input matching, meaning the ration of the input wave is back to the input port. The S11 curve shows that the input reflections in the emission band are below the required level of -16dB. One could then conclude that since the filter is resistive the response is symmetric, i.e., S11 and S22 are equal, as are S21 and S12, so that S12 and S22 do not need to be considered separately and they are in the specifications.

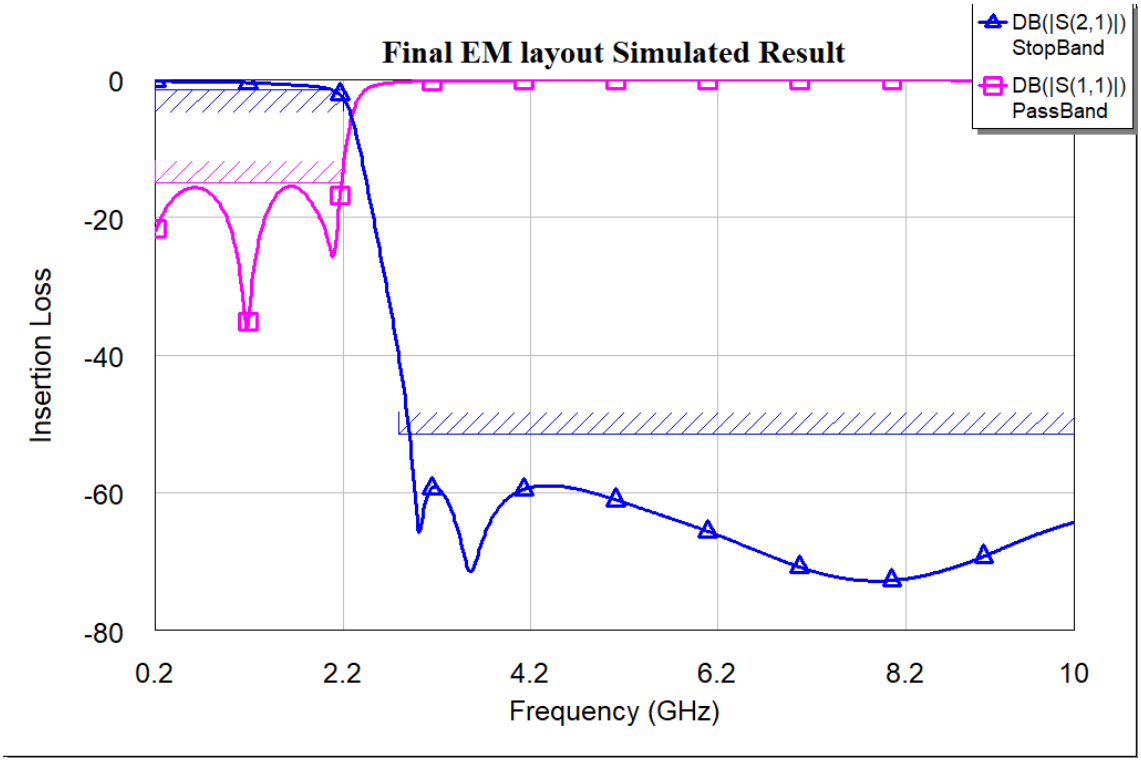

Figure 28. Final EM layout Simulated Model of the lowpass Filter Chebyshev.

5 Conclusion

This thesis work aimed to design a low-pass filter approached with Chebyshev response in IPD technology. There were specific specifications with pass-band frequency range of 2.2GHz, a ripple of 1.0dB, and an insertion loss of 1.5dB. The requirement for S11 in the emission band was-16dB. The stop-band frequency range was set between 2.8 and 10GHz, and suppression of 50dB relative to the pass-band edge.

The design was approached with a Chebyshev filter, the schematic was synthesized with Nuhertz Software and simulated and tuned in AWR software. The next step was to replace the central theoretical components of the schematic with the corresponding EM components, in order to create the EM-components to match the lumped components correspondently. Creating the component subcircuits was a crucial step to achieve the first layout model on

the EM-layout side. The EM-layout was created, and adjustments were needed to accomplish the design prototype. The iteration method was important in these adjustments for the design to be accomplish. The iteration method corrections were made by adding ports on every component at the EM-layout side and transferring it to a new blank page as a subcircuit. In this subcircuit, were added into every port lumped component either capacitors or inductors, in order to match the EM-layout side. This method helped to adjust the values by the tuning tool, but the values were not 100% absolute due to the passive components and Em-components differences. The final EM-layout was created with the adjustable values of the iteration method, and at the same time different size values were created named “decrease” or “increase” as a result of approaching the specifications.

The low-pass filter prototype matched the given specifications and achieved the goal. The prototype was sent to different partners who have been involved in this project. Also, the prototype achieved the design with IPD technology, which could be a valuable knowledge for VTT future’s projects. The next step is to process wafers for measurements and check the results of them. Finally, these given specifications could be approach by different type of filter, such as the Elliptic filter type, which could be more complicated and demanding than Chebyshev type.

References

1 Horowitz, Paul & Hill, Winfield (1989). *The Art of Electronics*, (2nd). New York: Cambridge University Press.

2 Jr., Hayt, William H. et al. (2002). *Engineering Circuit Analysis,* (6th). New York: R. R. Donnelley & Sons Company.

3 'The Circuit ad Filters Handbook' Chen, Wai-Kai (2009). (ed.) *Passive Active, and Digital Filters*, (3rd). University of Illinois Chicago: CRC Press, Taylor & Francis Group.

4 Mersereau, Russell M. & Jackson, Joel R. (2006). *Circuit Analysis: A System Approach*. USA: Pearson Prentice Hall.

5 Ludvig, Reinhold & Bretchko, Pavel (2000). *RF Circuit Design: Theory and Applications*. USA: Prentice-Hall.

6 Free, Charles E. & Aitchison, Colin S. (2022). *RF and Microwave Circuit Design: Theory and Applications*. UK: John Wiley & Sons Ltd.

7 Darwazeh, Izzat & Poole, Clive (2016). Microwave Active Circuit Analysis and Design. UK: Elsevier Ltd.

8 Pramanick, Protap & Bhartia, Prakash (2016). *Modern RF and Microwave Filter Design*. Canada: Artech House

9 Thede Les (2004). *Practical Analog and Digital Filter Design*. Ohio: Artech House.

10 Morgan A., Matthew (2017). *Reflectionless Filters*. University of Virginia: Artech House.

11 Lee H., Thomas (1998). *The Design of CMOS RadioFrequency Integrated Circuits*. USA: Cambridge University Press

12 Yang, Kai; He, Chenggong et al. (2023). Micro-Nanoelectronics*: Advanced RF Filters for Wireless Communications*. Volume 1 (2). 13-16. China: Hong Kong University of Science and Technology.

13 Liu, Kai; Lin, Yaojian (2007). A hybrid Coupled-Resonator Bandpass Filter Topology Implemented on Lossy Semiconductor Substrates. USA: Berkeley Height.